Current Biology 21, 53–58, January 11, 2011 ©2011 Elsevier Ltd All rights reserved DOI 10.1016/j.cub.2010.11.058

Report

Influence of Combinatorial Histone Modifications on Antibody and Effector Protein Recognition

Stephen M. Fuchs,[1,2] Krzysztof Krajewski,[1] Richard W. Baker,[1] Victoria L. Miller,[1] and Brian D. Strahl[1,2,*]

[1]Department of Biochemistry and Biophysics

[2]Lineberger Comprehensive Cancer Center

University of North Carolina School of Medicine, Chapel Hill, NC 27599, USA

Summary

Increasing evidence suggests that histone posttranslational modifications (PTMs) function in a combinatorial fashion to regulate the diverse activities associated with chromatin. Yet how these patterns of histone PTMs influence the adapter proteins known to bind them is poorly understood. In addition, how histone-specific antibodies are influenced by these same patterns of PTMs is largely unknown. Here we examine the binding properties of histone-specific antibodies and histone-interacting proteins using peptide arrays containing a library of combinatorially modified histone peptides. We find that modification-specific antibodies are more promiscuous in their PTM recognition than expected and are highly influenced by neighboring PTMs. Furthermore, we find that the binding of histone-interaction domains from BPTF, CHD1, and RAG2 to H3 lysine 4 trimethylation is also influenced by combinatorial PTMs. These results provide further support for the histone code hypothesis and raise specific concerns with the quality of the currently available modification-specific histone antibodies.

Results and Discussion

Protein posttranslational modifications (PTMs), such as phosphorylation, methylation, acetylation, and ubiquitination, regulate many processes, such as protein degradation, protein trafficking, and mediation of protein-protein interactions [1]. Perhaps the best-studied PTMs are those found to be associated with histone proteins. More than 100 histone PTMs have been described, and they largely function by recruiting protein factors to chromatin, which in turn drives processes such as transcription, replication, and DNA repair [2]. Likewise, dozens of chromatin-associating factors have been identified that bind to distinct histone PTMs, and hundreds of modification-specific histone antibodies have been developed to understand the in vivo function of these modifications [3, 4].

The enormous number of potential combinations of histone PTMs represents a major obstacle to our understanding of how PTMs regulate chromatin-templated processes, as well as to our ability to develop high-quality diagnostic tools for chromatin and epigenetic studies. The same obstacle applies to other proteins regulated by combinatorial PTMs: for example, p53, RNA polymerase, and nuclear receptors [5–7]. To that end, we developed a peptide array-based platform to begin to address how both histone-interacting proteins and antibodies recognize combinations of PTMs. We focused primarily on the recognition of PTMs associated with the N-terminal tail of histone H3, but this approach is useful for the study of other histone modifications and combinatorial PTMs found on other nonhistone proteins.

We generated a library of 110 synthetic histone peptides bearing either single or combinatorial PTMs and a biotin moiety for immobilization (Figure 1; see also Table S1 available online). Prior to printing, all peptides were subjected to rigorous quality control to verify their accuracy. This is significant because extensive peptide purification and mass spectrometric analysis is not possible with other recently described array technologies used to study combinatorial histone PTMs [8]. Another significant advancement in our method was the introduction of a biotinylated fluorescent tracer molecule, which served as a positive control for the quality of our printing in all experiments. Lastly, peptides were printed as a series of six spots, two times per slide by two different pins, yielding 24 independent measurements of every binding interaction per slide. These measures were adopted to minimize binding artifacts due to pin variation or inconsistencies on the slide surface. Thus, these arrays offer a large number of extensively characterized histone peptide substrates suitable for the assessment of effector protein or antibody binding.

We initially used our arrays to ask two fundamental questions regarding the recognition of histone PTMs: (1) How well do modification-directed antibodies recognize their intended epitope? and (2) What impact, if any, do combinatorial PTMs have on antibody recognition? We tested more than 20 commercially available antibodies raised against individual modifications on histone tails (see Tables S2 and S3 for information regarding antibodies and experimental conditions). Generally, we found that antibodies were reasonably proficient at recognizing their target modification (Figure S1). However, we found several exceptions, notably the discrimination between different methyllysine states by methyl-specific antibodies and the recognition of histone H3 lysine 14 acetylation (H3K14ac).

To explore methyllysine recognition, we tested the specificity of commercial antibodies raised against the three different methylated forms (mono-, di-, and trimethyl) of H3 at lysines 4 and 79 (H3K4me and H3K79me) (Figure 2). These antibodies were generally specific for their target lysine residue; however, both the trimethyl- and dimethyl-directed antibodies showed measurable cross-reactivity with dimethyllysine and monomethyllysine, respectively (Figure 2A and Figure S2). This finding has particular biological importance, because each methylation state of a given histone lysine residue is thought to mediate different biological outcomes through the recruitment of distinct chromatin-associated factors [9]. For example, H3K4me3 is well correlated with transcriptional activation through the recruitment of histone acetyltransferases and the preinitiation complex of transcription [10–12]. Conversely, H3K4me2 was reported to recruit the Set3 histone deacetylase complex [9]. The ability to distinguish between these methyl states is therefore necessary to dissect how H3K4 methylation controls the balance of histone acetylation and/or deacetylation at transcribed genes.

*Correspondence: brian_strahl@med.unc.edu

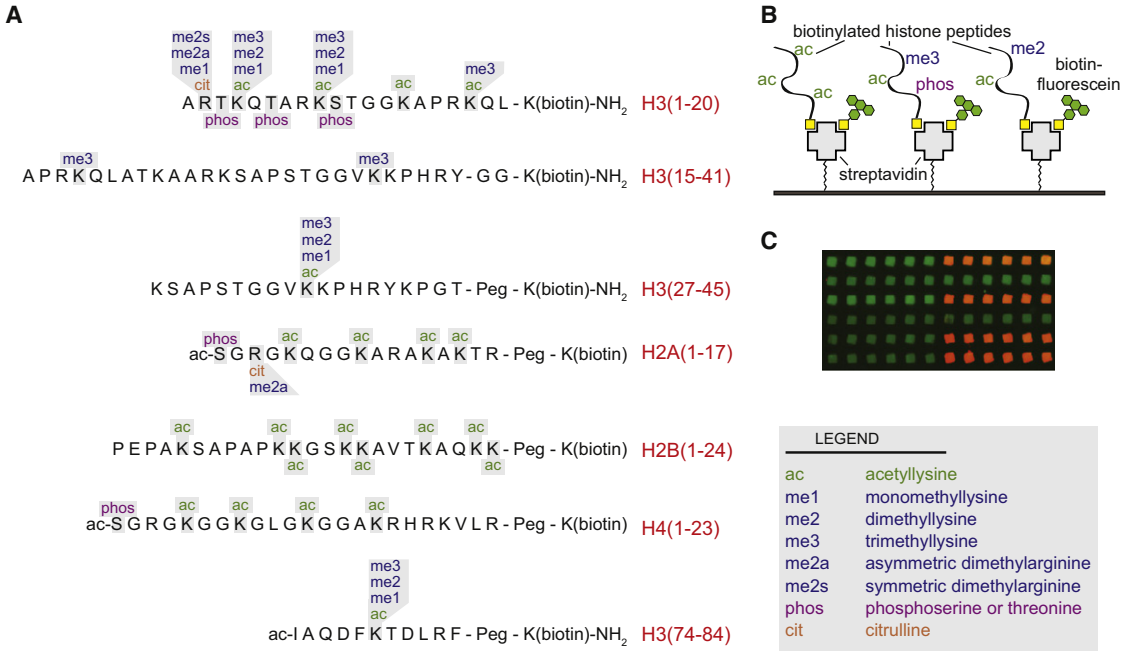

Figure 1. Composition of Histone Peptide Arrays

(A) Peptides synthesized for this study with possible side-chain modifications (in single or combinatorial fashion) are indicated for each amino acid.

(B) Depiction of array surface. Streptavidin-coated glass slides were spotted with a library of histone peptides containing different combinations of post-translational modifications (PTMs; see also Table S1 for complete peptide list). Biotin-fluorescein was mixed with the peptides and used as an internal control for spotting efficiency.

(C) Fluorescent image from a sample array. Positive binding interactions are shown as red spots where only the printing control (green) is visible for negative interactions.

We also tested a number of antibodies raised against acetyllysine found at position 14 of histone H3 (H3K14ac). Unlike lysine methylation, our arrays detected that several of these antibodies had difficulty in recognizing their target sequence, preferring acetylation at lysine 36 (H3K36ac) instead (Figure 2B). Additionally, peptide competition assays verified the interaction between the H3K14 antibodies and the H3K36ac peptide (Figure 2C). This result is likely explained by the fact that H3K14 and H3K36 are found in very similar sequence contexts and are acetylated by the same enzyme in vivo (Figure 2D). Acetylation of both H3K14 and H3K36 is catalyzed by the histone acetyltransferase Gcn5 [13]. However, H3K14ac is reported to be recognized by the RSC complex in yeast, whereas H3K36ac has been reported to be recognized by the bromodomain of PCAF in human cells [14, 15]. Thus, misdetection of H3K36ac using H3K14ac-directed antibodies by either western blot or chromatin immunoprecipitation may obscure our understanding of chromatin-templated processes regulated by H3K14 acetylation.

The large number of synthetic peptides containing combinatorial PTMs allowed us to additionally ascertain how PTM recognition is influenced by neighboring modifications. We therefore did further analysis of the H3K4me3 antibodies to determine how adjacent modifications affect substrate recognition. We observed that a monoclonal antibody widely used against H3K4me3 (Abcam; catalog number ab1012) is perturbed mainly by modification at histone H3 arginine 2 (H3R2) (Figure 3A). In contrast, a widely used polyclonal antibody from Millipore (catalog number 07-473) was negatively influenced by H3T6 phosphorylation, and a similar antibody from Active Motif (catalog number 39160) was not particularly sensitive to any neighboring modifications (Figure 3A).

We also examined the well-characterized PTM "switch" region on histone H3, where H3K9 is modified by either acetylation or methylation and where the neighboring serine 10 (H3S10) is a target for phosphorylation [16]. A polyclonal antibody (Active Motif; catalog number 39253) raised against H3S10 phosphorylation showed a statistically significant reduction in binding to peptides also modified at H3K9 (Figures 3B and 3C). In contrast, an antibody raised against both H3S10phos and H3K9ac (Cell Signaling; catalog number 9711) showed nearly absolute specificity for the peptide containing both modifications (Figures 3B and 3C). These data can be interpreted to suggest that biological changes in acetylation and methylation at H3K9 would influence the ability of antibodies derived against H3S10 phosphorylation to appropriately detect this mark. Such findings are significant, because H3S10 phosphorylation levels have already been found to change during the cell cycle and in response to histone deacetylase inhibitors [17–19].

Collectively, our analysis of histone PTM-specific antibodies enabled us to uncover recognition of related (but off-target) sequences in addition to adjacent PTM effects. This finding is significant because several major ongoing initiatives aimed at mapping and understanding how histone PTMs regulate biology, such as the National Institutes of Health (NIH) Epigenomic Roadmap and ENCODE, heavily rely on modification-specific antibodies [20].

In addition to being a powerful diagnostic tool for the characterization of PTM-derived antibodies, we used our peptide array technology to measure how PTM codes affect the interaction of chromatin-associated proteins. Accordingly, we measured the binding of several domains known to interact with H3K4me3. We found that the PHD domain from the V(D)J

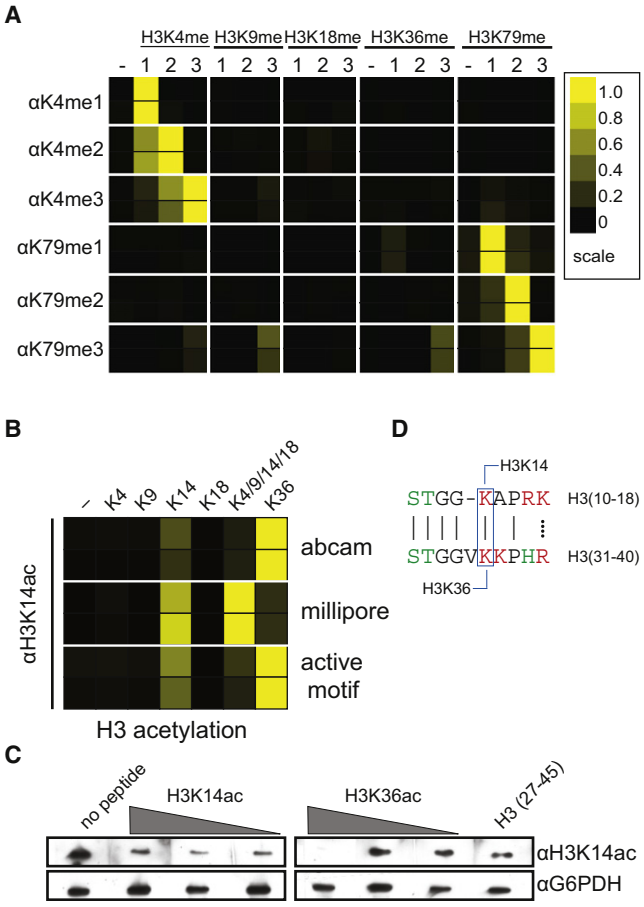

Figure 2. Antibody Binding to Histone Peptide Microarrays

Results of two independent arrays consisting of 24 independent spots for each peptide are depicted as heat maps of the normalized mean intensity and plotted on a scale from 0 to 1, with 1 (yellow) being the most significant (see Experimental Procedures).

(A) Interactions of H3K4- and H3K79-specific antibodies with methylated peptides derived from the N terminus of histone H3 (antibodies used are given in Table S1, and further information is given in Figures S1 and S3).

(B) Recognition of histone H3 acetyllysine peptides by H3K14ac antibodies.

(C) Western blot of yeast whole-cell extract probed with H3K14ac antibody preincubated with various concentrations of histone H3 peptides.

(D) Alignment of sequence surrounding H3K14 and H3K16.

recombination factor RAG2 was specific for H3K4me3 and was blocked by phosphorylation at either H3T3 or H3T6 (Figure 4A). From the structure of the RAG2 PHD domain bound to H3K4me3 peptide [21], it can clearly be seen how H3T3 phosphorylation may disrupt binding. Varier and coworkers very recently published that H3T3 phosphorylation acts as a switch to control the binding of TAF3 PHD domain [22]. Thus, this may be a general mechanism for controlling gene expression during mitosis (when H3T3 is phosphorylated). Similarly, Garske and coworkers found that H3T6 phosphorylation may disrupt RAG2 binding [23].

We next examined the tandem bromo-PHD domains of BPTF (subunit of the NURF ATP-dependent remodeling complex [24]). Our studies showed that the tandem domain was specific for H3K4me3 and also showed reduced binding in the presence of either H3T3 or H3T6 phosphorylation (Figure 4B). However, both RAG2 and BPTF are blocked by citrulline, but not by methylation at position 2, suggesting a role for the positive charge of H3R2 in PHD domain binding. Notably, converting H3R2 to citrulline results in a loss of cationic charge and likely loss of ionic and hydrogen bonding interactions within the pockets of the two PHD domains (Figures 4A and 4B). Interestingly, our ability to synthesize and print long peptides ($\geq$20 amino acids) allowed us to observe greater interactions of BPTF (PHD-bromo) with H3K4me3 peptides also harboring acetylation. We found that multiple acetylations on H3 enhanced the binding of BPTF to H3K4me3 (Figure 4B and Figure S3), suggesting coordination between the methyl-binding PHD domain and the acetyl-binding bromodomain to recognize multiple modifications on the histone H3 tail.

The chromodomain of human CHD1 is also known to recognize H3K4me3 but has a structurally distinct binding pocket from the PHD domains. We found that CHD1, like RAG2 and BPTF, preferentially binds H3K4me3 and is also negatively influenced by phosphorylation at H3T3 and H3T6 (Figure 4C). Interestingly, we also found that methylation of H3R2 appears to slightly enhance binding of CHD1, whereas citrullination at position 2 blocks this binding. Although the finding that H3R2 methylation reduces binding affinity of human CHD1 to H3K4me3 is in opposition to a previous report [25], this discrepancy may be due to the fact that Flanagan and coworkers used peptides labeled at the N terminus with fluorescein in their binding studies, which may have contributed to the binding. Consistent with our CHD1 findings, we and others have found that H3R2 methylation does not decrease CHD1 binding to H3K4me3 by either isothermal titration calorimetry (data not shown) or fluorescence polarization using C-terminally labeled peptides (Marcey Waters, personal communication). H3R2 methylation and H3K4me3 have been found to be mutually exclusive in yeast and humans [26, 27]. Thus, H3R2 methylation and H3K4me3 may function in specific circumstances to prevent the binding of effector proteins that promote gene transcription while facilitating the recruitment of CHD1 (and possibly other factors) to genes in order to promote gene silencing.

In conclusion, the complex patterns of histone PTMs are critical determinants of chromatin structure and function, but they also represent a significant challenge for future study. Although many protein domains that bind selectively to particular PTMs have been identified, little is known regarding how neighboring modifications inhibit or contribute to these interactions. Of equal importance is our understanding of how patterns of PTMs influence antibody recognition. In this case, detection of biologically important events could be blocked or misrepresented if neighboring modifications interfere with epitope recognition. Thus, our work underscores a need for more rigorous testing and characterization of histone-specific antibodies. Similar antibody concerns have been recently highlighted by other groups [20, 28]. The data sets for the antibodies and proteins described here, plus numerous additional antibodies, are available in Figure S1 and from our website (http://www.med.unc.edu/~bstrahl/Arrays/index.htm). In addition, we will continue to characterize histone antibody specificities and post the data to our website as an ongoing resource for the chromatin community.

Finally, although several other peptide array approaches have been used to measure binding to histone PTMs [8, 29–31], our arrays and assay approaches offer several advantages. First, our array displays a large number of peptides carrying multiple PTMs that are fully characterized by high-performance liquid chromatography (HPLC) and mass spectrometry (MS). Second, we take advantage of a biotin tracer molecule to provide an assessment of printing efficiency.

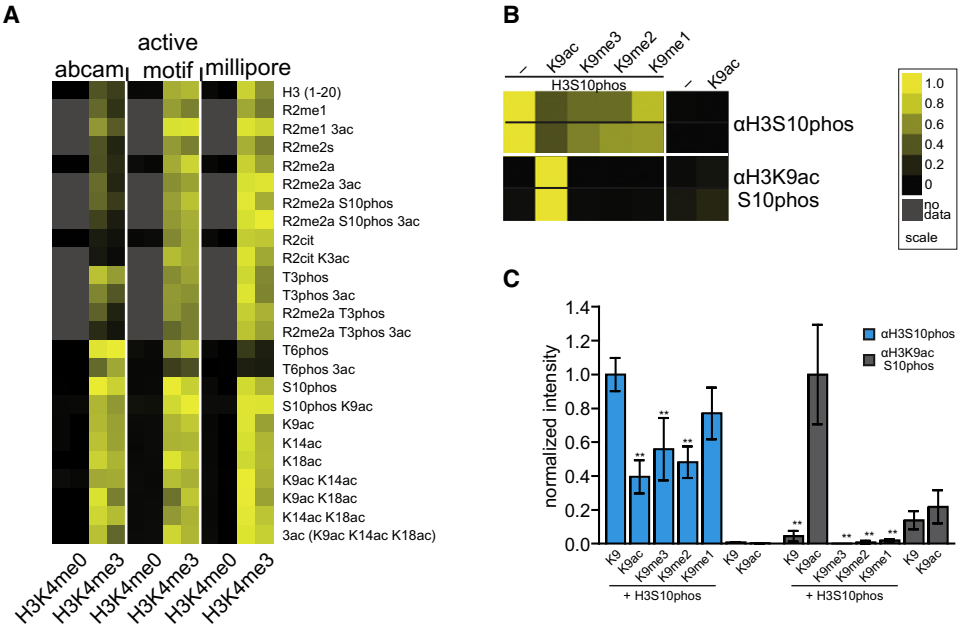

Figure 3. Effect of Neighboring Modifications on Histone Antibody Recognition

Results of two independent arrays consisting of 24 independent spots for each peptide are depicted as heat maps of the normalized mean intensity and plotted on a scale from 0 to 1, with 1 (yellow) being the most significant (see Experimental Procedures).

(A) Heat map showing the effects of neighboring modifications on H3K4me3-specific antibody recognition. 3ac = K9ac, K14ac, and K18ac.

(B) Recognition of H3S10 phosphorylation by mono- and dual-specific PTM antibodies.

(C) Bar graph of data in (B). Differences in intensities were compared using two-way analyses of variance, and confidence intervals (99% [**]) are indicated for individual comparisons. Further information is available in Figure S3.

Lastly, the high density of spotting allows us to perform statistical analysis of binding interactions. Although Liu et al. recently reported a similarly semiquantitative approach, their arrays were largely limited to peptides containing single PTMs, and the peptides were labeled via their N terminus, which could potentially occlude proteins and antibodies from recognizing modifications such as H3K4 methylation [30]. Furthermore, cellulose SPOT synthesis technology is limited by the inability to analytically characterize peptides [28]. In addition, a very elegant bead-based approach has been used to generate even larger peptide libraries and successfully characterize the binding of several protein factors to combinatorial histone PTMs [23]. However, our approach offers advantages in that we obtain binding data for each individual peptide and do not require sophisticated MS for the analysis. Regardless, several technologies now exist to enable the development of PTM-specific antibodies with better specificity. Furthermore, these technologies are useful for understanding how combinations of PTMs coordinate protein-protein interactions. This has important implications not only for chromatin biologists but also for those who study the role of PTMs in other systems [32].

Experimental Procedures

Antibodies

All primary antibodies tested are commercially available and are listed in Table S2. Secondary antibodies were Alexa Fluor 647 conjugated goat anti-rabbit IgG (catalog number A21244) and Alexa Fluor 647 conjugated rabbit anti-mouse IgG (catalog number A21239) antibodies from Invitrogen.

Peptide Synthesis

All reagents were obtained from commercial suppliers (AnaSpec, EMD, and Apptec). The peptides, biotinylated at their C termini, were synthesized on either NovaPEG Rink amide resin (histone H3 peptides) or Biotin-PEG NovaTag resin (histone H2A, H2B, and H4 peptides) using fluorenylmethyloxycarbonyl (Fmoc) chemistry on a PS-3 automated peptide synthesizer (see Table S1 for the complete list of peptides). All standard amino acids were coupled using HATU and N-methylmorpholine in dimethylformamide (DMF). Fmoc deprotection was performed using 20% piperidine in DMF. Modified amino acid residues were coupled using HATU, HOAt, and N,N,-diisopropyletylamine in NMP, and the coupling of these residues was monitored using ninhydrin test and repeated when needed. Peptides were cleaved from the resins using a 2.5% TIS and 2.5% water in trifluoroacetic acid (TFA). After TFA evaporation and washing with diethyl ether, the peptides were lyophilized from an acetonitrile/water solution and purified via preparative HPLC using water-acetonitrile gradient (0.1% TFA in both solvents) on a Waters SymmetryShield RP-18 5 μm 19 × 150 mm column. All peptides were analyzed using matrix-assisted laser desorption/ionization time-of-flight mass spectrometry and analytical HPLC. The average purity of peptides was over 90% (analytical HPLC). Analytical data for all peptides mentioned in this paper is available on our website.

Array Fabrication

Biotinylated peptides (25 μM final concentration) in printing buffer (10 mg/ml bovine serum albumin [BSA, Amresco], 0.3% Tween-20, and 10 μM biotin-conjugated fluorescein added to 1× ArrayIt protein printing buffer) were arrayed onto SuperStreptavidin-coated slides (ArrayIt) using SMP6 stealth pins (~200 μm spot diameter) and were arrayed onto OmniGrid100 arrayer (Digilab/Genomic Solutions) at ambient temperature and humidity (50%–60%) using the following printing parameters. To minimize effects from individual pins or localized imperfections in the substrate arrays, we arrayed samples as a series of six spots, two times on each slide at a spacing of 375 μm, as indicated in Table S4, and each peptide was printed by two different pins on each slide. After printing, slides were incubated overnight at 4°C in a humidified environment to facilitate interaction between the biotinylated peptide and the streptavidin surface. Slides were then blocked for 1 hr at 4°C with biotin-blocking buffer (ArrayIt), washed three times with phosphate-buffered saline (PBS), dried with air, stored at 4°C, and used within 60 days.

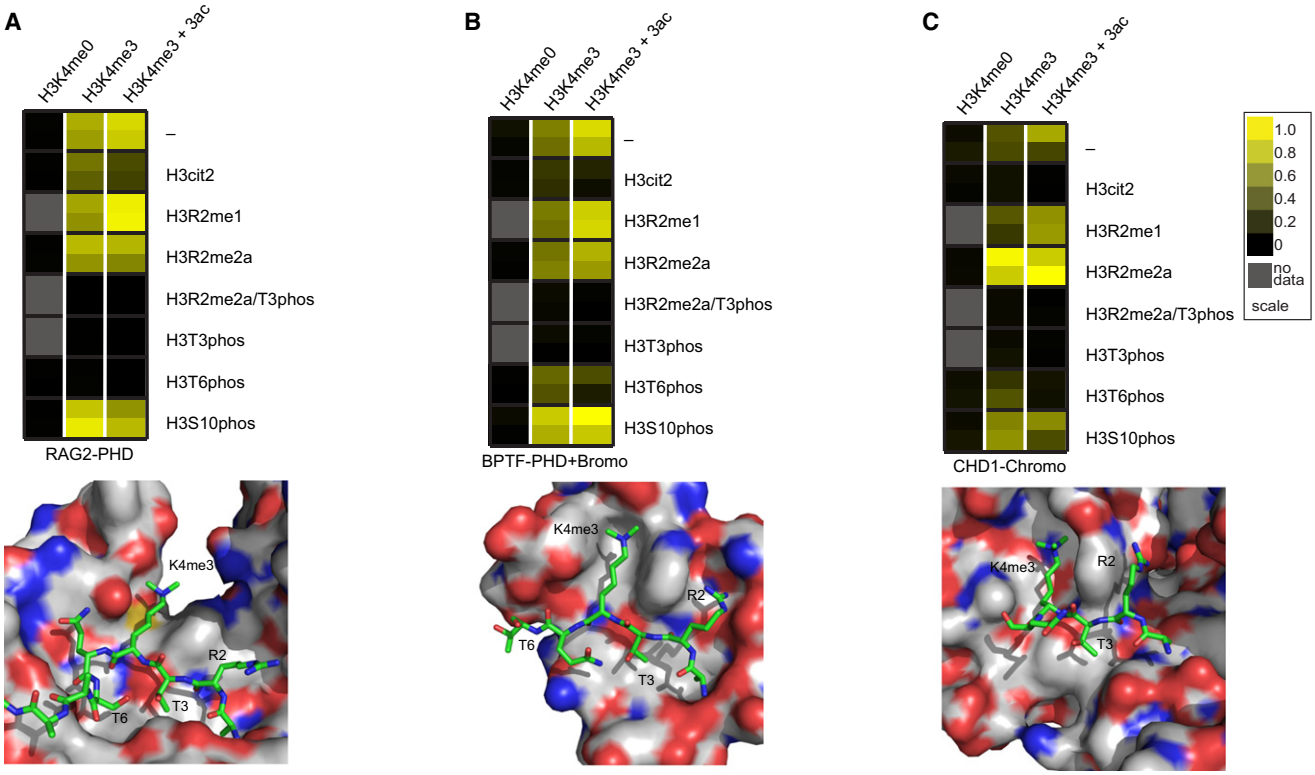

Figure 4. Chromatin-Associating Domain Binding to Histone Peptide Arrays

(A) Top: heat map of RAG2 PHD domain binding to histone H3 peptides. Bottom: molecular representation of the RAG2 PHD domain binding to an H3K4me3-containing peptide (PDB accession 2V83).

(B) Top: heat map of RAG2 PHD-Bromo domain binding to histone H3 peptides. Bottom: molecular representation of the BPTF PHD domain binding to an H3K4me3-containing peptide (PDB accession 2F6J).

(C) Top: heat map of CHD1 chromodomain binding to histone H3 peptides. Bottom: molecular representation of the CHD1 chromodomain binding to an H3K4me3-containing peptide (PDB accession 2B2W).

All models were constructed using PyMol software. Additional information is available in Figures S3 and S4.

Antibody Binding

Antibody dilutions were made in PBS containing 1% BSA (~10 mg/ml) and 0.3% Tween-20; the exact concentration for each array is summarized in Table S3. Antibodies were incubated with printed slides for 90–180 min at 4°C (with the exception of the H3K4me3 monoclonal antibody from Abcam, which was incubated overnight) and washed three times with cold PBS. Arrays were then probed with the appropriate Alexa Fluor 647 conjugated secondary antibody (Invitrogen) for 30–60 min at 4°C, washed three times with cold PBS, and dried. Arrays were then scanned using a Typhoon TRIO+ imager (GE Healthcare) at 10 μm resolution using the 526 nm and 670 nm filter sets for the biotin-fluorescein and secondary antibody, respectively. Interactions were quantified using ImageQuant array software (GE Healthcare).

Protein Expression

The chromatin-associating domains from mouse RAG2 (PHD 387–493), human BPTF (Bromo and PHD domain 2583–2751), and CHD1 (chromodomain 251–467) were C-terminally fused to GST in pGEX-4T. Proteins were heterologously expressed in *E. coli* and purified by glutathione sepharose affinity chromatography in PBS buffer (50 mM phosphate, 150 mM NaCl, pH 7.6) on an AKTA purifier fast protein liquid chromatography system (GE Healthcare).

Protein Binding

Prior to binding, arrays were blocked in PBS containing 5% BSA (~50 mg/mL) and 0.3% Tween-20 for 1 hr at 4°C to reduce nonspecific binding. Glutathione S-transferase (GST)-tagged protein (~25 μM) in the same buffer was overlaid on each array (200 μl total volume) and incubated in a hybridization chamber at 4°C overnight. Slides were washed three times with cold PBS. Anti-GST primary antibody was incubated with slides for 90–180 min at 4°C and washed three times with cold PBS. Arrays were then probed with the Alexa Fluor 647 conjugated anti-rabbit secondary antibody (Invitrogen) for 30–60 min at 4°C, washed three times with cold PBS, and dried. Arrays were then scanned using a Typhoon TRIO+ imager (GE Healthcare) at 10 μm resolution using the 526 nm and 670 nm filter sets for the biotin-fluorescein and secondary antibody, respectively. Interactions were quantified using ImageQuant array software (GE Healthcare).

Statistical Analysis

Briefly, printing of individual spots was evaluated based on the intensity of the fluorescein-biotin cospotted with each peptide. Spots with control intensities of less than 5% of the average intensity for all peptides were labeled as "not spotted" and omitted from subsequent analysis. Data were treated as four individual subarrays to account for small changes in intensity across the slide, each subarray containing all 110 peptides spotted six times. Alexa Fluor 647 intensities (corresponding to a positive interaction) were normalized for all spots by dividing the intensity by the sum of all intensities within a subarray. The six spots for each peptide were averaged (outliers were removed using a Grubbs test) and treated as a single value for a given subarray. The normalized intensities for the four subarrays were used to calculate the mean, and the error is reported as the standard error of the mean. For data displayed as heat maps, mean values were normalized to either the highest calculated value across all peptides or against the peptide for which a given antibody was supposed to interact. Heat maps were created using Java Treeview, and all data were plotted on a scale from 0 to 1 (Figure S1). Full data sets for all experiments are available at http://www.med.unc.edu/~bstrahl/Arrays/index.htm. Statistical analyses were performed using GraphPad Prism software. Analyses of variance were used to compare interactions, and confidence intervals are reported as 95% (*), 99% (**), or 99.9% (***).

Supplemental Information

Supplemental Information includes four figures and four tables and can be found with this article online at doi:10.1016/j.cub.2010.11.058.

Acknowledgments

This work was supported by an NIH EUREKA award to B.D.S. and an NIH National Research Service Award Postdoctoral Fellowship (GM80896) to S.M.F. The authors would like to thank Gary Johnson for use of the mass spectrometer, David Klapper for assistance with peptide synthesis, Andrew Nobel for suggestions with statistical analysis, Danny Reinberg and Patricia Cortes for providing us with GST expression plasmids, and Kathryn Gardner, Michael Keogh, Jorge Martinez, and Scott Rothbart for critical reading of this manuscript.

Received: October 20, 2010
Revised: November 19, 2010
Accepted: November 23, 2010
Published online: December 16, 2010

References

1. Walsh, C.T., Garneau-Tsodikova, S., and Gatto, G.J., Jr. (2005). Protein posttranslational modifications: The chemistry of proteome diversifications. Angew. Chem. Int. Ed. Engl. *44*, 7342–7372.
2. Kouzarides, T. (2007). Chromatin modifications and their function. Cell *128*, 693–705.
3. Ruthenburg, A.J., Allis, C.D., and Wysocka, J. (2007). Methylation of lysine 4 on histone H3: intricacy of writing and reading a single epigenetic mark. Mol. Cell *25*, 15–30.
4. Seet, B.T., Dikic, I., Zhou, M.M., and Pawson, T. (2006). Reading protein modifications with interaction domains. Nat. Rev. Mol. Cell Biol. *7*, 473–483.
5. Fuchs, S.M., Laribee, R.N., and Strahl, B.D. (2009). Protein modifications in transcription elongation. Biochim. Biophys. Acta *1789*, 26–36.
6. Meek, D.W., and Anderson, C.W. (2009). Posttranslational modification of p53: Cooperative integrators of function. Cold Spring Harb Perspect Biol *1*, a000950.
7. Perissi, V., and Rosenfeld, M.G. (2005). Controlling nuclear receptors: The circular logic of cofactor cycles. Nat. Rev. Mol. Cell Biol. *6*, 542–554.
8. Zhang, Y., Jurkowska, R., Soeroes, S., Rajavelu, A., Dhayalan, A., Bock, I., Rathert, P., Brandt, O., Reinhardt, R., Fischle, W., and Jeltsch, A. (2010). Chromatin methylation activity of Dnmt3a and Dnmt3a/3L is guided by interaction of the ADD domain with the histone H3 tail. Nucleic Acids Res. *38*, 4246–4253.
9. Kim, T., and Buratowski, S. (2009). Dimethylation of H3K4 by Set1 recruits the Set3 histone deacetylase complex to 5′ transcribed regions. Cell *137*, 259–272.
10. Hung, T., Binda, O., Champagne, K.S., Kuo, A.J., Johnson, K., Chang, H.Y., Simon, M.D., Kutateladze, T.G., and Gozani, O. (2009). ING4 mediates crosstalk between histone H3 K4 trimethylation and H3 acetylation to attenuate cellular transformation. Mol. Cell *33*, 248–256.
11. Taverna, S.D., Ilin, S., Rogers, R.S., Tanny, J.C., Lavender, H., Li, H., Baker, L., Boyle, J., Blair, L.P., Chait, B.T., et al. (2006). Yng1 PHD finger binding to H3 trimethylated at K4 promotes NuA3 HAT activity at K14 of H3 and transcription at a subset of targeted ORFs. Mol. Cell *24*, 785–796.
12. Vermeulen, M., Mulder, K.W., Denissov, S., Pijnappel, W.W., van Schaik, F.M., Varier, R.A., Baltissen, M.P., Stunnenberg, H.G., Mann, M., and Timmers, H.T. (2007). Selective anchoring of TFIID to nucleosomes by trimethylation of histone H3 lysine 4. Cell *131*, 58–69.
13. Morris, S.A., Rao, B., Garcia, B.A., Hake, S.B., Diaz, R.L., Shabanowitz, J., Hunt, D.F., Allis, C.D., Lieb, J.D., and Strahl, B.D. (2007). Identification of histone H3 lysine 36 acetylation as a highly conserved histone modification. J. Biol. Chem. *282*, 7632–7640.
14. Kasten, M., Szerlong, H., Erdjument-Bromage, H., Tempst, P., Werner, M., and Cairns, B.R. (2004). Tandem bromodomains in the chromatin remodeler RSC recognize acetylated histone H3 Lys14. EMBO J. *23*, 1348–1359.
15. Zeng, L., Zhang, Q., Gerona-Navarro, G., Moshkina, N., and Zhou, M.M. (2008). Structural basis of site-specific histone recognition by the bromodomains of human coactivators PCAF and CBP/p300. Structure *16*, 643–652.
16. Fischle, W., Wang, Y., and Allis, C.D. (2003). Binary switches and modification cassettes in histone biology and beyond. Nature *425*, 475–479.
17. Davies, G.F., Ross, A.R., Arnason, T.G., Juurlink, B.H., and Harkness, T.A. (2010). Troglitazone inhibits histone deacetylase activity in breast cancer cells. Cancer Lett. *288*, 236–250.
18. Hayashi-Takanaka, Y., Yamagata, K., Nozaki, N., and Kimura, H. (2009). Visualizing histone modifications in living cells: Spatiotemporal dynamics of H3 phosphorylation during interphase. J. Cell Biol. *187*, 781–790.
19. Zhang, X., Zhang, Z., Chen, G., Zhao, M., Wang, D., Zhang, X., Du, Z., Xu, Y., and Yu, X. (2010). FK228 induces mitotic catastrophe in A549 cells by mistargeting chromosomal passenger complex localization through changing centromeric H3K9 hypoacetylation. Acta Biochim. Biophys. Sin. (Shanghai) *42*, 677–687.
20. Egelhofer, T.A., Minoda, A., Klugman, S., Lee, K., Kolasinska-Zwierz, P., Alekseyenko, A.A., Cheung, M.-S., Day, D.S., Gadel, S., Gorchakov, A.A., et al. (2010). An assessment of histone-modification antibody quality. Nat. Struct. Mol. Biol., in press. 10.1038/10.1038/nsmb.1972.
21. Ramón-Maiques, S., Kuo, A.J., Carney, D., Matthews, A.G., Oettinger, M.A., Gozani, O., and Yang, W. (2007). The plant homeodomain finger of RAG2 recognizes histone H3 methylated at both lysine-4 and arginine-2. Proc. Natl. Acad. Sci. USA *104*, 18993–18998.
22. Varier, R.A., Outchkourov, N.S., de Graaf, P., van Schaik, F.M., Ensing, H.J., Wang, F., Higgins, J.M., Kops, G.J., and Timmers, H.M. (2010). A phospho/methyl switch at histone H3 regulates TFIID association with mitotic chromosomes. EMBO J, in press. Published online October 15, 2010. 10.1038/emboj.2010.261.
23. Garske, A.L., Oliver, S.S., Wagner, E.K., Musselman, C.A., LeRoy, G., Garcia, B.A., Kutateladze, T.G., and Denu, J.M. (2010). Combinatorial profiling of chromatin binding modules reveals multisite discrimination. Nat. Chem. Biol. *6*, 283–290.
24. Li, H., Ilin, S., Wang, W., Duncan, E.M., Wysocka, J., Allis, C.D., and Patel, D.J. (2006). Molecular basis for site-specific read-out of histone H3K4me3 by the BPTF PHD finger of NURF. Nature *442*, 91–95.
25. Flanagan, J.F., Mi, L.Z., Chruszcz, M., Cymborowski, M., Clines, K.L., Kim, Y., Minor, W., Rastinejad, F., and Khorasanizadeh, S. (2005). Double chromodomains cooperate to recognize the methylated histone H3 tail. Nature *438*, 1181–1185.
26. Guccione, E., Bassi, C., Casadio, F., Martinato, F., Cesaroni, M., Schuchlautz, H., Lüscher, B., and Amati, B. (2007). Methylation of histone H3R2 by PRMT6 and H3K4 by an MLL complex are mutually exclusive. Nature *449*, 933–937.
27. Kirmizis, A., Santos-Rosa, H., Penkett, C.J., Singer, M.A., Vermeulen, M., Mann, M., Bähler, J., Green, R.D., and Kouzarides, T. (2007). Arginine methylation at histone H3R2 controls deposition of H3K4 trimethylation. Nature *449*, 928–932.
28. Bock, I., Dhayalan, A., Kudithipudi, S., Brandt, O., Rathert, P., and Jeltsch, A. (2011). Detailed specificity analysis of antibodies binding to modified histone tails with peptide arrays. Epigenetics *6*, 256–263.
29. Bua, D.J., Kuo, A.J., Cheung, P., Liu, C.L., Migliori, V., Espejo, A., Casadio, F., Bassi, C., Amati, B., Bedford, M.T., et al. (2009). Epigenome microarray platform for proteome-wide dissection of chromatin-signaling networks. PLoS ONE *4*, e6789.
30. Liu, H., Galka, M., Iberg, A., Wang, Z., Li, L., Voss, C., Jiang, X., Lajoie, G., Huang, Z., Bedford, M.T., and Li, S.S. (2010). Systematic identification of methyllysine-driven interactions for histone and nonhistone targets. J. Proteome Res. *9*, 5827–5836.
31. Matthews, A.G., Kuo, A.J., Ramón-Maiques, S., Han, S., Champagne, K.S., Ivanov, D., Gallardo, M., Carney, D., Cheung, P., Ciccone, D.N., et al. (2007). RAG2 PHD finger couples histone H3 lysine 4 trimethylation with V(D)J recombination. Nature *450*, 1106–1110.
32. Sims, R.J., 3rd, and Reinberg, D. (2008). Is there a code embedded in proteins that is based on post-translational modifications? Nat. Rev. Mol. Cell Biol. *9*, 815–820.